

Heterostructures of transition metal dichalcogenides

B. Amin, N. Singh, and U. Schwingenschlög^{*}

KAUST, Physical Science & Engineering Division, Thuwal 23955-6900, Kingdom of Saudi Arabia

(Received 27 April 2015; published 24 August 2015)

The structural, electronic, optical, and photocatalytic properties of out-of-plane and in-plane heterostructures of transition metal dichalcogenides are investigated by (hybrid) first principles calculations. The out-of-plane heterostructures are found to be indirect band gap semiconductors with type-II band alignment. Direct band gaps can be achieved by moderate tensile strain in specific cases. The excitonic peaks show blueshifts as compared to the parent monolayer systems, whereas redshifts occur when the chalcogen atoms are exchanged along the series S-Se-Te. Strong absorption from infrared to visible light as well as excellent photocatalytic properties can be achieved.

DOI: [10.1103/PhysRevB.92.075439](https://doi.org/10.1103/PhysRevB.92.075439)

PACS number(s): 73.22.-f

I. INTRODUCTION

Transition metal dichalcogenide (TMDC, MX_2 with $M = \text{Mo, W}$ and $X = \text{S, Se, and Te}$) monolayers are emerging as promising materials for a wide range of applications, e.g., in energy storage [1], gas sensors [2], catalysis [3], field-effect transistors [4], and optoelectronic/photonic devices [5]. Due to their distinct properties, they also have been put forward for logic circuits [6] and memory devices [7]. It has been demonstrated that quantum confinement in MoS_2 results in indirect-to-direct band gap crossover [8] and enhanced photocatalytic activity [9,10]. In general, the properties of TMDC monolayers can be tuned by doping [11], alloying [12], strain engineering [13], stacking [14], and the formation of superlattices [15]. Optical band gaps ranging from the near infrared to the visible light region and strong light-matter interaction enable the development of efficient photovoltaic devices based on TMDC monolayer heterostructures [16].

In-plane and out-of-plane MoS_2 - WS_2 heterostructures have been grown and characterized by both Raman and photoluminescence spectroscopy [17]. Excitonic transitions at 1.4 eV in the photoluminescence spectra of the out-of-plane heterostructures later could not be reproduced and therefore have been attributed to the substrate [18]. Thickness and stacking effects on the phonon spectra of MoS_2 and WS_2 monolayers and their out-of-plane heterostructures have been addressed by first principles calculations in Ref. [19]. The heterostructures exhibit indirect band gaps, as do the corresponding bulk compounds [19,20]. On the other hand, MoS_2 - WS_2 and MoS_2 - MoTe_2 in-plane heterostructures are subject to significant modifications of the electronic properties as compared to the corresponding pure monolayer systems [21,22].

The Coulomb interaction in TMDC monolayers results in strongly bound excitons [23]. While in bulk TMDCs the excitons have binding energies of less than 100 meV, e.g., 40 meV in MoS_2 , in the monolayer systems these energies can be ten times larger [11]. This offers new opportunities for exciton engineering and paves the way to optoelectronic applications. Engineering the generation, dissociation, transfer, and recombination of excitons by the formation of heterostructures

is also of fundamental importance in photovoltaics [24]. Long-lived interlayer excitons in out-of-plane MoSe_2 - WSe_2 heterostructures have been reported recently in Ref. [25]. Indeed, similar lattice parameters allow the creation of a variety of TMDC heterostructures with very few structural defects [26]. However, despite their technological relevance [27] and various results from first principles calculations [28–30], the properties that can be expected from such systems are still under debate. In particular, the nature of the band gap (direct versus indirect) of the MoSe_2 - WSe_2 and MoTe_2 - WTe_2 heterostructures is not settled [31]. In the present work, we therefore provide an accurate description of the electronic structure in terms of hybrid functional calculations. In addition, we present a comparative study of excitonic effects in TMDC heterostructures and analyze possible applications in photocatalysis.

II. COMPUTATIONAL DETAILS

We employ density functional theory in the projector augmented plane wave scheme [32]. Using the Perdew-Burke-Ernzerhof (PBE) functional, we relax the heterostructures taking into account the van der Waals interaction by the empirical dispersion correction proposed by Grimme [33]. This procedure yields good agreement with experiments with respect to the interlayer distance. The plane wave cutoff is set to 500 eV and the atomic positions are relaxed until the forces have converged to 10^{-3} eV/Å and the energy to 10^{-4} eV. Γ -centered Monkhorst-Pack k-meshes are employed for integrating the Brillouin zone. We use for the structural relaxation $6 \times 6 \times 2$ and $6 \times 6 \times 1$ k-meshes for the out-of-plane and in-plane heterostructures, respectively, which are refined to $12 \times 12 \times 4$ and $12 \times 12 \times 1$ for the optimized structures. A vacuum layer thicker than 16 Å prevents artifacts of the periodic boundary conditions in the out-of-plane direction. The effect of spin-orbit coupling is significant for both Mo and W and hence is taken into account in all calculations.

The converged PBE wave functions are used as starting points for hybrid functional Heyd-Scuseria-Ernzerhof (HSE06) calculations [34]. Due to the high computational costs associated with this method the k-mesh here is not refined. In addition, we employ the GW_0 approach, where the HSE06 single particle energies and wave functions are used to calculate the quasiparticle energies. The HSE06 wave

^{*}Udo.Schwingenschlogl@kaust.edu.sa

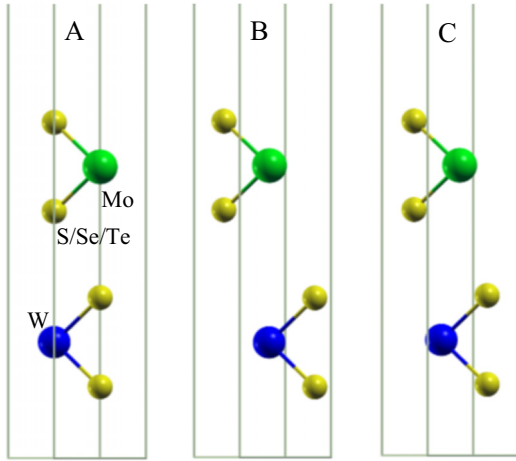


FIG. 1. (Color online) Out-of-plane heterostructures for different stackings.

functions are also used to solve the Bethe-Salpeter equation (Tamm-Dancoff approximation) in order to study the optical spectrum. We take into account the 10 highest valence and 10 lowest conduction bands for calculating the excitonic eigenstates.

III. RESULTS AND DISCUSSION

In our out-of-plane heterostructures we use the in-plane lattice constants obtained by optimization of the involved monolayer systems. Moreover, we approximate the orthorhombic structure of WTe_2 as hexagonal for the sake of comparison with the other compounds. Since the electronic structure is very sensitive to the layer stacking [31], we study various choices; see Fig. 1. A: the X atoms of one monolayer are located on top of the M atoms of the other layer, similar to the most stable phase of bulk TMDCs [35]. B: the M atoms are located on top of each other, which is the second layer stacking known from bulk TMDCs. C: the two monolayers are shifted laterally so that on-top positions are avoided. The binding energy, given by the total energies of the heterostructure and the two isolated monolayer systems,

$$E = E_{\text{MoX}_2\text{-WX}_2} - E_{\text{MoX}_2} - E_{\text{WX}_2}, \quad (1)$$

shows that stacking A is favorable in each case; see Table I. Therefore, this situation is studied in the following. By its only slightly higher energy, stacking B should still be accessible in

TABLE I. Formation energy and interlayer distance for the out-of-plane heterostructures.

Stacking A	$\text{MoS}_2\text{-WS}_2$	$\text{MoSe}_2\text{-WSe}_2$	$\text{MoTe}_2\text{-WTe}_2$
E (eV)	-0.20	-0.26	-0.38
d (Å)	6.16	6.48	6.94
Stacking B	$\text{MoS}_2\text{-WS}_2$	$\text{MoSe}_2\text{-WSe}_2$	$\text{MoTe}_2\text{-WTe}_2$
E (eV)	-0.18	-0.24	-0.32
d (Å)	6.20	6.62	7.20
Stacking C	$\text{MoS}_2\text{-WS}_2$	$\text{MoSe}_2\text{-WSe}_2$	$\text{MoTe}_2\text{-WTe}_2$
E (eV)	-0.14	-0.20	-0.24
d (Å)	6.29	6.65	7.30

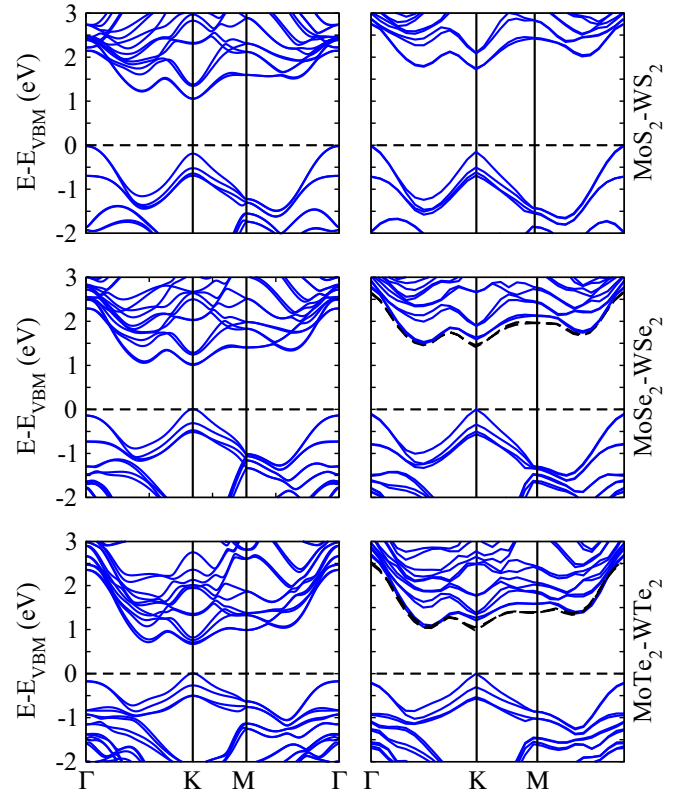


FIG. 2. (Color online) Band structures of the out-of-plane heterostructures obtained using the PBE (left) and HSE06 (right) functionals. The black dashed conduction bands are obtained under strain; see the text for details.

experiment, whereas stacking C is practically not relevant. The interlayer distances obtained for stacking A turn out to be in agreement with experimental values of MoS_2 (6.15 Å), WS_2 (6.16 Å), MoSe_2 (6.45 Å), and WSe_2 (6.49 Å) bilayer systems [35].

The PBE band structure in Fig. 2 (top left) shows that the $\text{MoS}_2\text{-WS}_2$ heterostructure has an indirect band gap with the valence band maximum (VBM) at the Γ point and the conduction band minimum (CBM) at the K point, in agreement with experiment [18] and theoretical reports [19]. In contrast to the experimental situation [25], the $\text{MoSe}_2\text{-WSe}_2$ and $\text{MoTe}_2\text{-WTe}_2$ heterostructures show direct band gaps; see Fig. 2 (middle and bottom left) and Ref. [31]. The PBE functional also underestimates the band gap values [25]; see Table II. In order to improve the accuracy, we therefore use the HSE06 functional. The results in Fig. 2 (right) show for all heterostructures the expected indirect band gap. The larger the M-X bond length, the smaller the splitting of the bonding and antibonding states and thus the band gap [36]. Hence Table II demonstrates significant potential for band gap engineering by stacking TMDC monolayers. In general, mechanical strain is one of the most prominent approaches to manipulate the band structure [37]. Indeed, we find for moderate in-plane tensile strain of 0.75% ($\text{MoSe}_2\text{-WSe}_2$) and 1.5% ($\text{MoTe}_2\text{-WTe}_2$) a shifting of the CBM to the K point, i.e., a direct band gap; see the black dashed conduction bands in Fig. 2 (right). On

TABLE II. Band gaps and splittings of the valence and conduction bands for the out-of-plane heterostructures.

PBE	MoS ₂ -WS ₂	MoSe ₂ -WSe ₂	MoTe ₂ -WTe ₂
E_g (eV)	1.2	1.0	0.7
Δ_{VB} (meV)	342	324	278
Δ_{CB} (meV)	3	21	37
HSE06	MoS ₂ -WS ₂	MoSe ₂ -WSe ₂	MoTe ₂ -WTe ₂
E_g (eV)	1.7	1.5	1.1
Δ_{VB} (meV)	364	354	304
Δ_{CB} (meV)	22	43	63
GW ₀	MoS ₂ -WS ₂	MoSe ₂ -WSe ₂	MoTe ₂ -WTe ₂
E_g (eV)	2.1	1.8	1.3

the other hand, the MoS₂-WS₂ heterostructure maintains its indirect band gap nature under any reasonable tensile strain.

The orbitally weighted HSE06 band structures for the out-of-plane heterostructures in Fig. 3 show that the CBM at the K point is due to the Mo $d_{3z^2-r^2}$ states, while the VBM at the Γ point is due to the W $d_{3z^2-r^2}$ states. This kind of localization of the VBM and CBM in different regions of the heterostructure spatially separates electron-hole pairs (type-II band alignment), which is useful for light detection and harvesting, because no additional material is needed for this purpose [22,38]. TMDC bilayers do not possess this property, so that an external electric field is required to achieve a type-II band alignment [39]. Moreover, strong spin-orbit

TABLE III. Splittings of the valence and conduction bands in TMDC monolayers.

PBE	MoS ₂	MoSe ₂	MoTe ₂	WS ₂	WSe ₂	WTe ₂
Δ_{VB} (meV)	143	179	205	409	460	465
Δ_{CB} (meV)	2	22	36	4	8	46
HSE06	MoS ₂	MoSe ₂	MoTe ₂	WS ₂	WSe ₂	WTe ₂
Δ_{VB} (meV)	156	193	220	439	510	512
Δ_{CB} (meV)	20	44	67	15	54	60

coupling results in significant valence and conduction band splittings ($\Delta_{VB/CB}$), see Table II, where the value of Δ_{CB} obtained for the MoSe₂-WSe₂ heterostructure agrees well with the experiment [25]. In each case, the splittings are stronger than in the pristine MoX₂ monolayer and weaker than in the pristine WX₂ monolayer; see the monolayer results in Table III. We note that the HSE06 functional tends to overestimate Δ_{VB} in TMDC monolayers [40], which is likely to be the case for heterostructures as well. The fact that the Mo $d_{3z^2-r^2}$ states dominate at the CBM explains why the Δ_{CB} values of the heterostructures are close to those of the corresponding MoX₂ monolayers. The possibility to engineer the valence and conduction band splittings by means of the composition of a heterostructure is important for the field of spintronics, since these quantities are related to the spin relaxation time.

We further have calculated the imaginary part of the dielectric function, $\epsilon_2(\omega)$, of the monolayer systems and heterostructures by solving the Bethe-Salpeter equation. The results in Fig. 4 show that the optical transitions are dominated by excitons. For monolayer MoS₂ excitonic peaks are observed at 1.65 eV and 1.85 eV, while for monolayer WS₂ they appear at 1.66 eV and 2.15 eV, in agreement with experiment [14,41] and previous calculations [23]. Figure 4 shows a systematic redshift of the excitonic peaks as the chalcogen atom becomes heavier. We obtain exciton binding energies of 0.95 eV for MoS₂, 0.70 eV for MoSe₂, 1.04 eV for WS₂, 1.01 eV for WSe₂, 0.80 eV for MoTe₂, and 0.66 eV for WTe₂ monolayers. Differences to Ref. [23] (1.03 eV for MoS₂, 0.91 eV for MoSe₂, 1.04 eV for WS₂, 0.90 eV for WSe₂, and 0.71 eV for MoTe₂ monolayers) can be explained by the less accurate calculation method used by these authors. The experimental exciton binding energy of WS₂ (reported values vary between 0.32 eV [42] and 0.83 eV [43]), on the other hand, is overestimated by at least 25% and a similar deviation applies also to MoSe₂, for which a value of 0.55 eV has been measured [44].

The excitonic peaks are shifted to 1.78 eV and 1.94 eV in the case of the MoS₂-WS₂ heterostructure, in agreement with photoluminescence spectroscopy [17,18]. We find no extra excitonic peak at 1.4 eV, which supports the conjecture of Ref. [18] mentioned before. For the MoSe₂-WSe₂ heterostructure the excitonic peaks at 1.40 eV and 1.70 eV also appear in the photoluminescence spectrum [25], while for the MoTe₂-WTe₂ heterostructure no experimental data are available for comparison. Figure 4 demonstrates strong modifications of the excitons in the heterostructures with respect to the parent monolayer systems. Interlayer excitons previously have been reported for molecular donor/acceptor interfaces in the context of organic photovoltaics [45,46]. They have smaller optical dipoles than

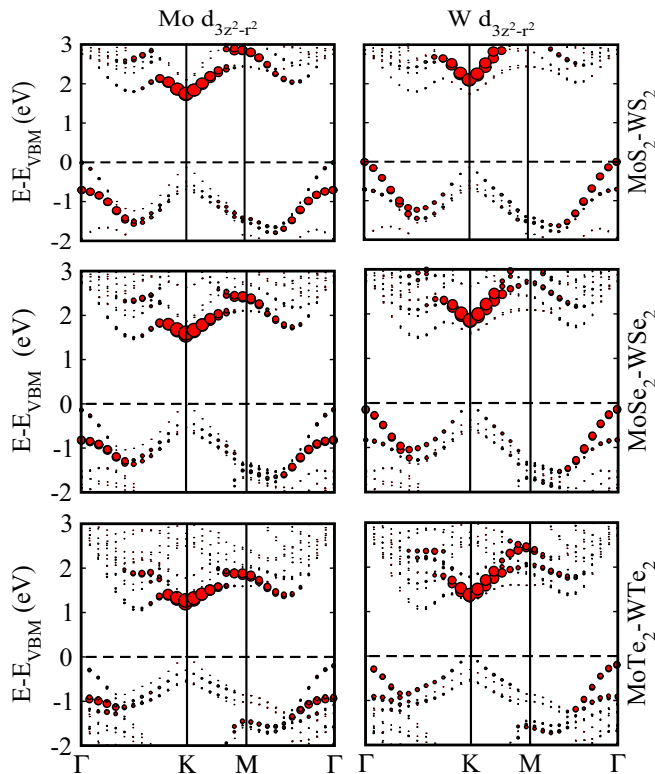


FIG. 3. (Color online) Orbitally weighted HSE06 band structures of the out-of-plane heterostructures, taking into account the spin-orbit coupling.

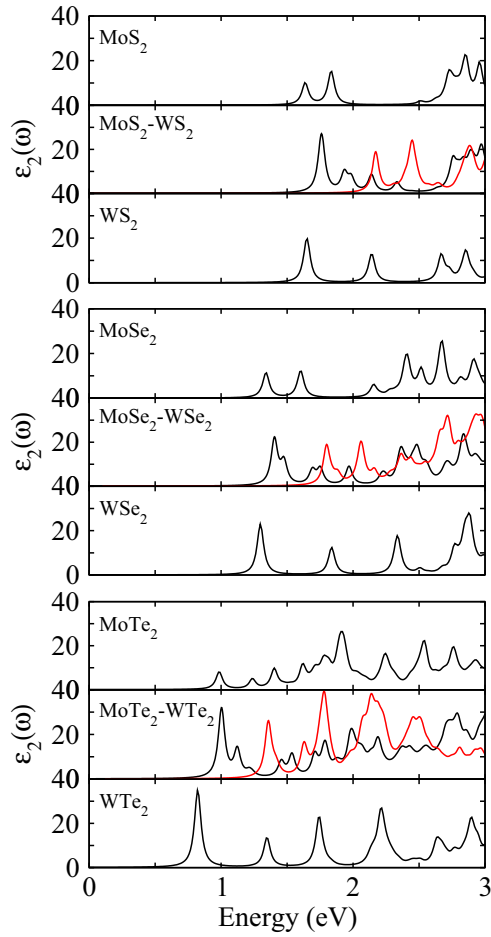


FIG. 4. (Color online) Imaginary part of the dielectric function of the out-of-plane (black) and in-plane (red) heterostructures as compared to the parent monolayer systems.

intralayer excitons and longer recombination lifetimes (about one order of magnitude) of nanoseconds, which are useful in optoelectronics and laser applications. Indeed, we obtain smaller exciton binding energies of 0.40 eV, 0.36 eV, and 0.34 eV for the MoS₂-WS₂, MoSe₂-WSe₂, and MoTe₂-WTe₂ heterostructures, respectively, than for the monolayer systems.

In order to study grain boundaries in TMDC monolayers, we address the in-plane heterostructure shown in Fig. 5, which

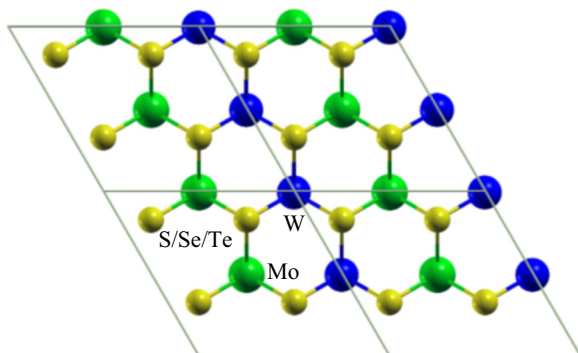


FIG. 5. (Color online) In-plane heterostructures.

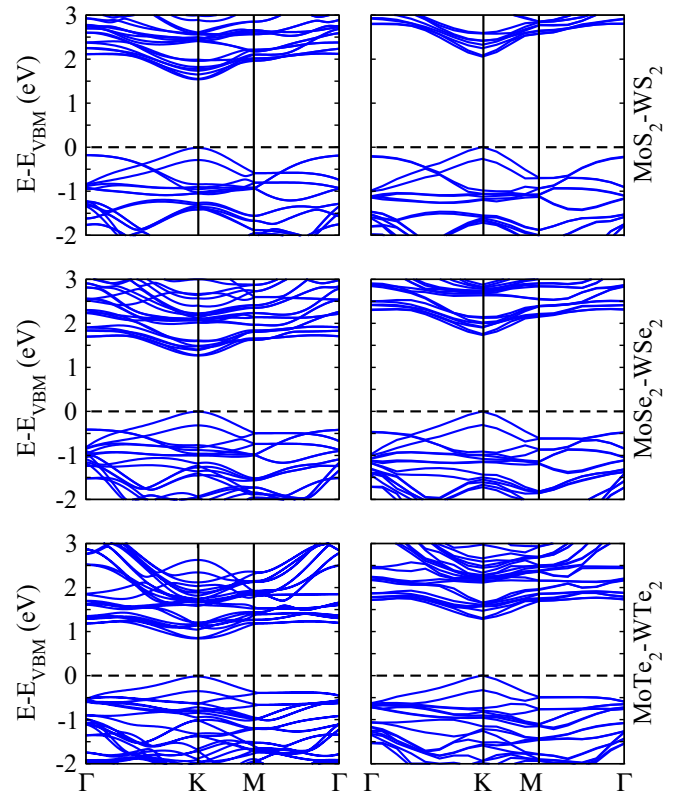


FIG. 6. (Color online) Band structures of the in-plane heterostructures obtained using the PBE (left) and HSE06 (right) functionals.

realizes the largest possible concentration of grain boundaries. The structure optimization yields only minor deviations from the pristine monolayers (W-X bond length changes by less than 1%) due to the structural similarity between MoX₂ and WX₂. All the in-plane heterostructures have direct band gaps, see Fig. 6, with the VBM and CBM at the K point. Although the nature of the band gap is correctly described by the PBE functional, the HSE06 functional improves its size and yields values in the visible range of the solar spectrum; see Table IV. Since PBE and GW₀ calculations substantially under and overestimate the band gaps of the monolayer

TABLE IV. Band gaps and splittings of the valence and conduction bands for the in-plane heterostructures.

PBE	MoS ₂ -WS ₂	MoSe ₂ -WSe ₂	MoTe ₂ -WTe ₂
E_g (eV)	1.5	1.3	0.8
Δ_{VB} (meV)	273	311	332
Δ_{CB} (meV)	14	11	10
HSE06	MoS ₂ -WS ₂	MoSe ₂ -WSe ₂	MoTe ₂ -WTe ₂
E_g (eV)	2.0	1.7	1.2
Δ_{VB} (meV)	283	324	337
Δ_{CB} (meV)	24	22	20
GW ₀	MoS ₂ -WS ₂	MoSe ₂ -WSe ₂	MoTe ₂ -WTe ₂
E_g (eV)	2.8	2.4	1.6

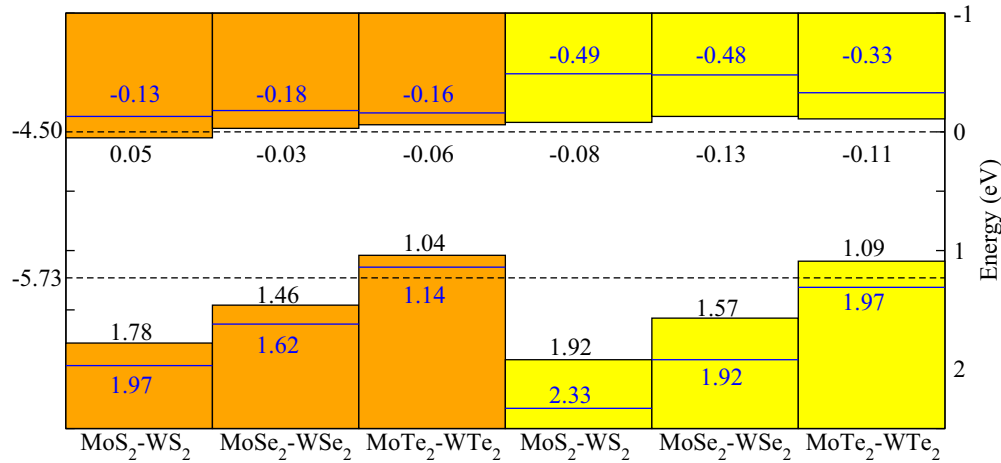


FIG. 7. (Color online) Valence and conduction band edge potentials for the out-of-plane (orange) and in-plane (yellow) heterostructures. The values are obtained by HSE06 (black) and GW_0 (blue) calculations. The dashed lines represent the water reduction (H^+/H_2) and oxidation (H_2O/O_2) potentials.

systems, respectively, we analyze in the following our HSE06 results.

We find contributions of both Mo and W to the CBM and VBM and thus a fundamentally different scenario than for the out-of-plane heterostructures (i.e., no type-II band alignment). The situation is also different to the MoS_2/BN heterostructure, where the energetic separation between the MoS_2 and BN states is much larger [12]. The heavier the chalcogenide atom the smaller the band gap, similar to the out-of-plane heterostructures. According to Table IV, the valence and conduction band splittings of the in-plane heterostructures are intermediate between those of the parent monolayer systems, which again opens the possibility of band structure engineering.

The optical properties of the in-plane heterostructures are addressed in Fig. 4 (red color). For all cases the excitonic peaks show blueshifts (the second peak being more pronounced) as compared to the out-of-plane heterostructures. The exciton binding energies (0.64 eV, 0.56 eV, and 0.34 eV for MoS_2-WS_2 , $MoSe_2-WSe_2$, and $MoTe_2-WTe_2$, respectively) lie in between those of the corresponding out-of-plane heterostructures and monolayer systems, reflecting again reduced Coulomb interaction. For the $MoTe_2-WTe_2$ heterostructure, in particular, a strong excitonic peak is observed in Fig. 4 near the optimal band gap of 1.4 eV for solar energy harvesting.

To investigate the photocatalytic properties of our heterostructures, we determine the energies of the VBM and CBM by means of the Mulliken electronegativity [47,48],

$$E_{VBM} = \chi - E_{elec} + 0.5E_g \quad \text{and} \quad E_{CBM} = E_{VBM} - E_g, \quad (2)$$

where E_{VBM} and E_{CBM} are the edge potentials, χ is the geometric mean of the electronegativities of the constituent atoms, and $E_{elec} = 4.5$ eV is the standard electrode potential on the hydrogen scale. The values of χ are 5.42 eV for MoS_2-WS_2 , 5.22 eV for $MoSe_2-WSe_2$, and 4.99 eV for $MoTe_2-WTe_2$. Figure 7 summarizes the edge potentials obtained by HSE06

and GW_0 calculations. For the MoS_2-WS_2 and $MoSe_2-WSe_2$ out-of-plane heterostructures E_{VBM} is higher than the H_2O/O_2 potential (1.23 eV) [47], showing that H_2O can be oxidized to O_2 . Moreover, the GW_0 results for E_{CBM} are lower than the H^+/H_2 potential (0 eV), showing that H^+ can be reduced to H_2 . The results are similar for the corresponding in-plane heterostructures, suggesting that they are likewise useful for photocatalysis. Both $MoTe_2-WTe_2$ heterostructures can reduce H^+ to H_2 but fail to oxidize H_2O to O_2 .

IV. CONCLUSION

We have investigated the structural, electronic, optical, and photocatalytic properties of transition metal dichalcogenide heterostructures. The stacking order of minimal energy has been determined for the out-of-plane heterostructures, which show indirect band gaps with type-II band alignment. Moderate tensile strain can be used to induce direct band gaps in the cases of the $MoSe_2-WSe_2$ and $MoTe_2-WTe_2$ heterostructures. All in-plane heterostructures have direct band gaps without type-II band alignment. Optical spectra demonstrate that bound excitons are responsible for the first optical transitions in all heterostructures, where the excitonic binding energies compare well to the available experimental data. Strong absorption of solar light makes the materials interesting for photovoltaic applications. In addition, both the out-of-plane and in-plane MoS_2-WS_2 and $MoSe_2-WSe_2$ heterostructures are suitable for photocatalysis.

ACKNOWLEDGMENTS

Research reported in this publication was supported by the King Abdullah University of Science and Technology (KAUST). We thank H. P. Komsa and T. P. Kaloni for fruitful discussions.

- [1] Y. Zhao, Y. Zhang, Z. Yang, Y. Yan, and K. Sun, *Sci. Technol. Adv. Mater.* **14**, 043501 (2013).
- [2] D. J. Late, Y.-K. Huang, B. Liu, J. Acharya, S. N. Shirodkar, J. Luo, A. Yan, D. Charles, U. V. Waghmare, V. P. Dravid, and C. N. R. Rao, *ACS Nano* **7**, 4879 (2013).
- [3] Y. Li, H. Wang, L. Xie, Y. Liang, G. Hong, and H. Dai, *J. Am. Chem. Soc.* **133**, 7296 (2011).
- [4] M. Chhowalla, H. S. Shin, G. Eda, L.-J. Li, K. P. Loh, and H. Zhang, *Nat. Chem.* **5**, 263 (2013).
- [5] K. Xu, Z. Wang, X. Du, M. Safdar, C. Jiang, and J. He, *Nanotechnology* **24**, 465705 (2013).
- [6] B. Radisavljevic, M. B. Whitwick, and A. Kis, *ACS Nano* **5**, 9934 (2011).
- [7] S. Bertolazzi, D. Krasnozhan, and A. Kis, *ACS Nano* **7**, 3246 (2013).
- [8] T. Georgiou, R. Jalil, B. D. Belle, L. Britnell, R. V. Gorbachev, S. V. Morozov, Y. Kim, A. Gholinia, S. J. Haigh, O. Makarovskiy, L. Eaves, L. A. Ponomarenko, A. K. Geim, K. S. Novoselov, and A. Mishchenko, *Nat. Nanotechnol.* **8**, 100 (2012).
- [9] M. A. Lukowski, A. S. Daniel, F. Meng, A. Forticaux, L. Li, and S. Jin, *J. Am. Chem. Soc.* **135**, 10274 (2013).
- [10] N. Singh, G. Jabbour, and U. Schwingenschlögl, *Eur. Phys. J. B* **85**, 392 (2012).
- [11] H. P. Komsa, J. Kotakoski, S. Kurasch, O. Lehtinen, U. Kaiser, and A. V. Krasheninnikov, *Phys. Rev. Lett.* **109**, 035503 (2012).
- [12] H. P. Komsa and A. V. Krasheninnikov, *Phys. Rev. B* **88**, 085318 (2013).
- [13] B. Amin, T. P. Kaloni, and U. Schwingenschlögl, *RSC Adv.* **4**, 34561 (2014).
- [14] X. Hong, J. Kim, S. F. Shi, Y. Zhang, C. Jin, Y. Sun, S. Tongay, J. Wu, Y. Zhang, and F. Wang, *Nat. Nanotechnol.* **9**, 682 (2014).
- [15] N. Lu, H. Guo, L. Wang, X. Wu, and X. C. Zeng, *Nanoscale* **6**, 4566 (2014).
- [16] L. Britnell, R. M. Ribeiro, A. Eckmann, R. Jalil, B. D. Belle, A. Mishchenko, Y.-J. Kim, R. V. Gorbachev, T. Georgiou, S. V. Morozov, A. N. Grigorenko, A. K. Geim, C. Casiraghi, A. H. Castro Neto, and K. S. Novoselov, *Science* **340**, 1311 (2013).
- [17] Y. Gong, J. Lin, X. Wang, G. Shi, S. Lei, Z. Lin, X. Zou, G. Ye, R. Vajtai, B. I. Yakobson, H. Terrones, M. Terrones, B. K. Tay, J. Lou, S. T. Pantelides, Z. Liu, W. Zhou, and P. M. Ajayan, *Nat. Mater.* **13**, 1135 (2014).
- [18] Y. Yu, S. Hu, L. Su, L. Huang, Y. Liu, Z. Jin, A. A. Purezky, D. B. Geohegan, K. W. Kim, Y. Zhang, and L. Cao, *Nano Lett.* **15**, 486 (2015).
- [19] L. Liang and V. Meunier, *Nanoscale* **6**, 5394 (2014).
- [20] M. Bernardi, M. Palummo, and J. C. Grossman, *Nano Lett.* **13**, 3664 (2013).
- [21] Q. Wang, P. Wu, G. Cao, and M. Huang, *J. Phys. D: Appl. Phys.* **46**, 505308 (2013).
- [22] J. Kang, S. Tongay, J. Zhou, J. Li, and J. Wu, *Appl. Phys. Lett.* **102**, 012111 (2013).
- [23] A. Ramasubramaniam, *Phys. Rev. B* **86**, 115409 (2012).
- [24] G. Weisbuch and B. Vinter, *Quantum Semiconductor Structures: Fundamentals and Applications* (Academic Press, San Diego, 1991).
- [25] P. Rivera, J. R. Schaibley, A. M. Jones, J. S. Ross, S. Wu, G. Aivazian, P. Klement, N. J. Ghimire, J. Yan, D. G. Mandrus, W. Yao, and X. Xu, *Nat. Commun.* **6**, 6242 (2015).
- [26] P. Johari and V. B. Shenoy, *ACS Nano* **6**, 5449 (2012).
- [27] N. Perea-López, A. L. Elías, A. Berkdemir, A. Castro-Beltrán, H. R. Gutiérrez, S. Feng, R. Lv, T. Hayashi, F. López-Urías, S. Ghosh, B. Muchharla, S. Talapatra, H. Terrones, and M. Terrones, *Adv. Funct. Mater.* **23**, 5511 (2013).
- [28] X. Su, R. Zhang, C.-F. Guo, M. Guoc, and Z. Rena, *Phys. Chem. Chem. Phys.* **16**, 1393 (2014).
- [29] M. Sharma, A. Kumar, P. K. Ahluwalia, and R. Pandey, *J. Appl. Phys.* **116**, 063711 (2014).
- [30] K. Kosmider and J. Fernández-Rossier, *Phys. Rev. B* **87**, 075451 (2013).
- [31] H. Terrones, F. Lopez-Urías, and M. Terrones, *Sci. Rep.* **3**, 1549 (2013).
- [32] G. Kresse and J. Hafner, *Phys. Rev. B* **47**, 558 (1993).
- [33] S. Grimme, *J. Comput. Chem.* **27**, 1787 (2006).
- [34] J. Heyd, G. E. Scuseria, and M. Ernzerhof, *J. Chem. Phys.* **124**, 219906 (2006).
- [35] J. He, K. Hummer, and C. Franchini, *Phys. Rev. B* **89**, 075409 (2014).
- [36] C. H. Chang, X. Fan, S. H. Lin, and J. L. Kuo, *Phys. Rev. B* **88**, 195420 (2013).
- [37] N. Lu, H. Guo, L. Li, J. Dai, L. Wang, W. N. Mei, X. Wu, and X. C. Zeng, *Nanoscale* **6**, 2879 (2014).
- [38] X. L. Wei, H. Zhang, G. C. Guo, X. B. Li, W. M. Lau, and L. M. Liu, *J. Mater. Chem. A* **2**, 2101 (2014).
- [39] A. Ramasubramaniam, D. Naveh, and E. Towe, *Phys. Rev. B* **84**, 205325 (2011).
- [40] A. Kormányos, G. Burkard, M. Gmitra, J. Fabian, V. Zólyomi, N. D. Drummond, and V. Fal'ko, *2D Mater.* **2**, 022001 (2015).
- [41] K. F. Mak, C. Lee, J. Hone, J. Shan, and T. F. Heinz, *Phys. Rev. Lett.* **105**, 136805 (2010).
- [42] A. Chernikov, T. C. Berkelbach, H. M. Hill, A. Rigosi, Y. Li, O. B. Aslan, D. R. Reichman, M. S. Hybertsen, and T. F. Heinz, *Phys. Rev. Lett.* **113**, 076802 (2014).
- [43] A. T. Hanbicki, M. Currie, G. Kioseoglou, A. L. Friedman, and B. T. Jonker, *Solid State Commun.* **203**, 16 (2015).
- [44] M. M. Ugeda, A. J. Bradley, S.-F. Shi, F. H. da Jornada, Y. Zhang, D. Y. Qiu, W. Ruan, S.-K. Mo, Z. Hussain, Z.-X. Shen, F. Wang, S. G. Louie, and M. F. Crommie, *Nat. Mater.* **13**, 1091 (2014).
- [45] A. E. Jaiilaubekov, A. P. Willard, J. R. Tritsch, W.-L. Chan, N. Sai, R. Gearba, L. G. Kaake, K. J. Williams, K. Leung, P. J. Rossky, and X.-Y. Zhu, *Nat. Mater.* **12**, 66 (2012).
- [46] S. Gelinas, A. Rao, A. Kumar, S. L. Smith, A. W. Chin, J. Clark, T. S. van der Poll, G. C. Bazan, and R. H. Friend, *Science* **343**, 512 (2013).
- [47] J. J. Liu, X. L. Fu, S. F. Chen, and Y. F. Zhu, *Appl. Phys. Lett.* **99**, 191903 (2011).
- [48] H. L. Zhuang and R. G. Hennig, *Phys. Rev. B* **88**, 115314 (2013).